Cracks in porous rocks: Tiny defects, strong effects

YVES GUÉGUEN, JOËL SAROUT, JÉRÔME FORTIN, and ALEXANDRE SCHUBNEL, Ecole Normale Supérieure

Understanding the physics and mechanics of porous sedimentary rocks is a stimulating challenge. Indeed, these rocks are of great economical interest for two main reasons: they are the places for hydrocarbon resources and for underground storage. Yet the complexity of these natural composites would suggest low expectations for research projects aiming at a fundamental understanding of their behavior. However progress has been observed, not limited to the study of pure quartz sandstones such as Fontainebleau sandstones. Many experiments and models have been developed that deal with more typical, complex sandstones. Even shales, that are certainly the most complex sedimentary rocks, have also been well documented. But why is it of interest to understand better the fundamental physics and mechanics of sedimentary rocks? And how has progress been made possible, given those difficulties?

A first key reason that motivates the interest is subsidence: when depleted, hydrocarbon reservoirs may exhibit strong subsidence, as observed in the North Sea. The mechanical response to depletion is of major importance. A fundamental understanding of the micromechanics is required if quantitative predictions need to be made. Progresses have resulted from experimental investigation of compaction in sandstones that have shown that compaction can be localized or not. This, obviously, raises the question of permeability: how does compaction affect permeability?

A second key reason behind the current research is passive and active monitoring: microseismic activity and elastic wave velocities provide a way to monitor the reservoir and/or the overlying layer. Hence a sufficiently good understanding of the processes could open the way to a reasonably reliable monitoring. Again experiments are providing results on acoustic emissions (pico-earthquakes that are heard at the laboratory scale) triggering and elastic wave velocity variations in controlled conditions. Progress relies on our ability to understand these results. Combining the measurement of acoustic emission monitoring, elastic wave velocity measurements with mechanical deformation seems to be a fruitful method in that case.

Compacting sandstones through dilatancy

Mechanical compaction and the associated porosity reduction in sandstones have been much investigated in the laboratory. Chemical compaction—a process dominant at depths greater than 4 km—is not considered here. Mechanical compaction may occur because production decreases the pore pressure. The "effective pressure P" is taken as the difference between the confining pressure Pc and the pore pressure Pp. The effective pressure is the controlling parameter for simple, hydrostatic (isotropic) loading. When submitted to hydrostatic loading, either in dry (Pp = 0) or in wet (Pp = 10 MPa) conditions, Bleurswiller sandstone (a Vosgian sandstone with an initial porosity of 25%) exhibits a sharp critical pressure P* beyond which inelastic porosity reduction takes place (Figure 1).

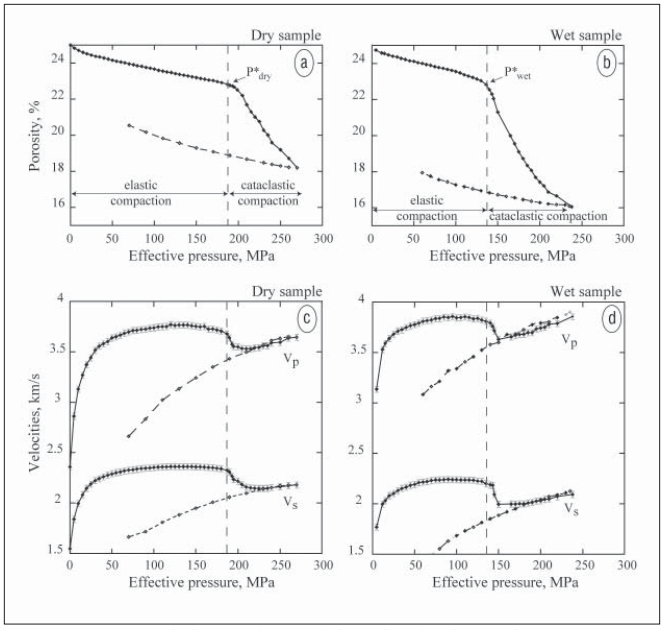

Figure 1. *(a) and (b) Mechanical data for the dry and wet specimens (Bleurswiller sandstone). The porosity reduction is plotted versus effective pressure. The critical pressure P* indicates the beginning of pore collapse and grain crushing. P* is lower in the wet specimen than in the dry specimen, which is explained by chemical weakening effects. The unloading is plotted as dashed lines. (c) and (d) Velocity measurements for the dry and wet specimens. The elastic wave velocities P and S are plotted versus the effective pressure. At the critical pressure P*, the velocities decrease because of grain crushing and pore collapse. Note that at pressure P ≈ 220 MPa and P ≈ 160 MPa, in the dry and wet specimens, respectively, the velocities increase again. The unloading is plotted as dashed lines. (from Fortin et al. 2007, Figure 7.)*

This behavior is typical of sandstones. The exact value of P* depends on the rock's mineralogical composition, its grain size, and its porosity. Note also that P* is strongly reduced in presence of water, as can be seen from Figure 1. The water effect can be explained by the fact that fracture energy is affected by water adsorption. Water adsorption decreases the surface and fracture energy, making cracking easier. Critical pressure P* is indeed the point where grain crushing—implying microcracking—takes place. Grain crushing makes pore collapse possible, so that irreversible porosity reduction begins when P = P*. The occurrence of microcracking implies that some (very small) dilatancy develops at P*. Porosity reduction resulting from pore collapse is larger than microcrack dilatancy by at least one order of magnitude, so that dilatancy is not visible in Figure 1a andb. Its existence is, however, firmly established from three independent observations. First, pore collapse requires microcracking to allow grain crushing, second post-mortem observations show the micro-cracks, and third, elastic wave velocities exhibit a strong decrease at P* (Figure 1, c and d). This last in-situ

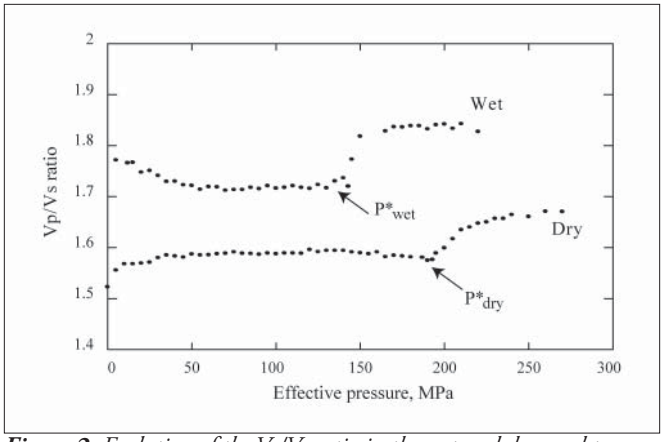

Figure 2. *Evolution of the V_P/V_S ratio in the wet and dry sandstone specimens as functions of effective pressure. Dots are experimental data. Note that at the pressure state P*, the ratio V_P/V_S increases both in the wet and dry cases. (from Fortin et al. 2007, Figure 11.)*

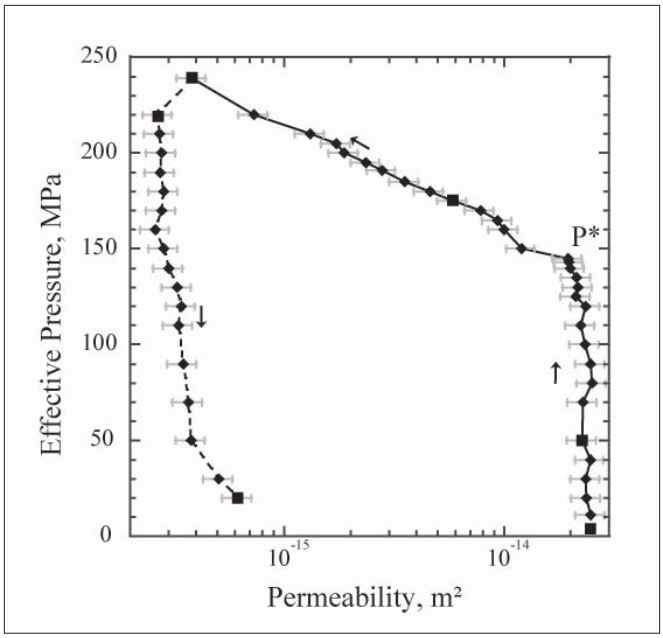

Figure 3. *Evolution of the permeability as a function of effective pressure. Permeability is almost constant up to P* and decreases continuously beyond this critical pressure. The unloading is plotted as dashed lines. (from Fortin et al. 2005, Figure 3b.)*

observation can be explained either in terms of cracks, or equivalently, in terms of the transformation of a solid matrix into a granular medium. For instance, the results of Figure 1 in the wet case are interpreted by the introduction of a crack density of 0.4 at P = P*.

Using effective elasticity and inverting both P and S-wave data, a second crack parameter—mean crack aspect ratio—is derived: this mean crack aspect ratio is found to be close to 10^{-3}. In terms of the V_P/V_S ratio, the results of Figure 2 indicate a jump from 1.72 to 1.82 (wet case) that implies an increase of the effective Poisson ratio. This is the commonly observed behavior for saturated cracked rocks. In the dry case, however, the V_P/V_S ratio increases as well at P* (Figure 2). This is not a classical result at all. It can nicely be interpreted through

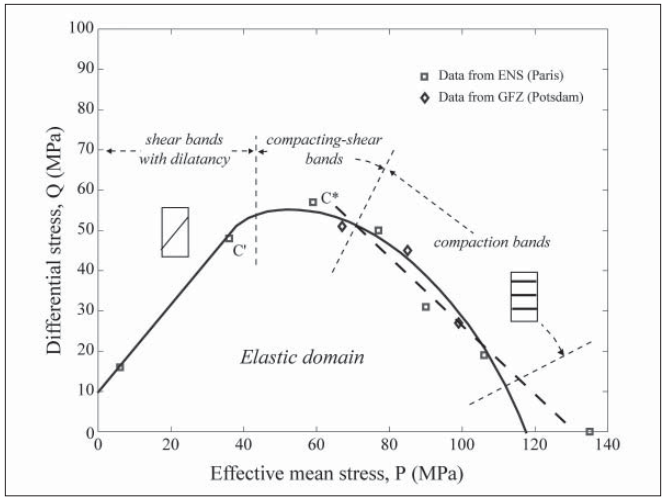

Figure 4. *Yield envelopes for brittle strength and shear-enhanced compaction: stress state C* at the onset of shear-enhanced compaction (effective confining pressure higher than 30MPa), and stress state C' at the onset of shear-induced dilatation for brittle fracture are shown in stress space. Note that the compactive yield envelope approximately follows a straight line with negative slope. (from Fortin et al. 2006), Figure 13.)*

a granular model: what is taking place is the destruction of the original cemented rock that is progressively transformed into a pack of uncemented grains. This process corresponds to a kind of lubrication, making the solid rock more fluid-like, and thus increasing its effective Poisson ratio, like in the wet case. As expected, permeability is almost constant up to P*. Beyond P*, permeability decreases continuously (Figure 3). The well-connected network of large pores is progressively destroyed and replaced by a network of low-aperture cracks. Overall, the rock compacts in an homogeneous way.

Anisotropic loading changes strikingly this behavior. The same Bleurswiller sandstone compacts at a critical effective pressure threshold C* that now also depends on differential stress Q. The typical observed trend for sandstones is similar to that of Figure 4, although some details may differ (Figure 4 shows a linear decrease of C* with increasing P, whereas some other sandstones may follow a more elliptical trend). The observed shear-enhanced compaction is not homogeneous: localized compaction bands are observed. The compaction bands are made of crushed grains and constitute permeability barriers. Passive recording of acoustic emissions (AE) agrees very well with post-mortem observations and confirms the formation of those compaction bands (Figure 5).

Energy radiated acoustically during crack propagation: Lithology and rupture speed effects

Recent advances in technology have lead to fast acoustic emission acquisition systems allowing new observations of rupture. Indeed, these new AE data acquisition systems enable the recording of continuous acoustic waveforms for significant time periods (up to one hour), and at a sampling frequency of 10 MHz, thus removing any sampling bias imposed by former triggering logics. In the laboratory, marble has been studied widely since it can undergo a brittle-plastic

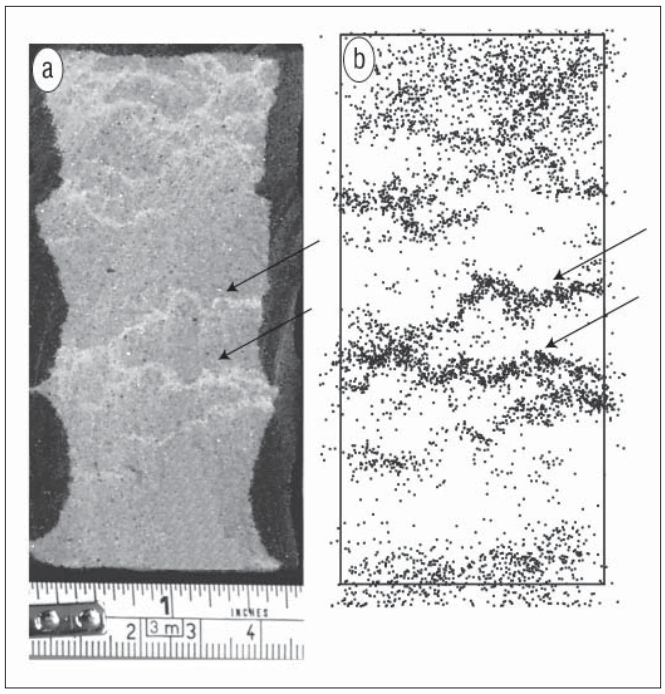

Figure 5. *Under an anisotropic loading, compaction bands can be observed. (a) is a picture of the longitudinal section of a deformed sample. Dark color indicates epoxy. Examples of compaction band are indicated by arrows. The direction of the maximal compression axis is vertical. In (b) the locations of all AE events recorded during the loading are plotted. Note that the AE hypocenter distribution shows excellent agreement with the location of deformation bands. (from Fortin et al. 2006, Figure10.)*

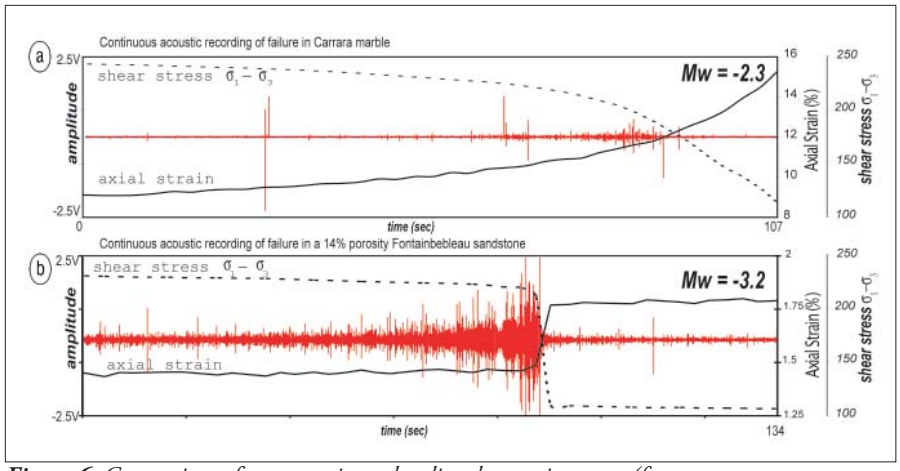

Figure 6. *Comparison of stress, strain and radiated acoustic energy (frequency range = 0.1-1MHz) in a marble and a sandstone. (a) In Carrara marble: evolution of axial strain, shear stress and acoustic activity (107 seconds segment of the continuous waveform recorded at failure) versus time. (b) In an intact 14% porosity Fontainebleau sandstone. (134 s continuous waveform recorded at failure). Stress scale is the same in (a) and (b), not strain scale. Moment magnitudes Mw were calculated from the mechanical data and are indicated for comparison. (from Schubnel et al., 2006; Figure 3, Schubnel et al. 2007, Figure 3.)*

transition at room temperature as calcite requires low shear stresses to initiate plastic processes: *r*-, *f*-dislocation glide, and twinning are activated even at room temperature. In such way, a number of studies have documented the mechanical behavior of Carrara marble. On the other hand, and as presented in the previous section, sandstones are typical of brittle behavior, because grain crushing takes place at the microscale even in the cataclastic flow regime. This is in particularly true with sandstones of low-to-medium porosity (ϕ <15%), and very rich in quartz such as Fontainebleau sandstone.

Figure 6 compares the continuous acoustic waveforms recorded at rupture for a sample of Carrara marble and a sample of Fontainebleau sandstone, both deformed in similar conditions. On top of the continuous acoustic waveforms are plotted the evolutions of stress and strain with time. The slips on the fracture plane triggered by rupture were ~1.5 mm and 0.2 mm respectively. For sake of comparison only, this would correspond to moment magnitudes MW of approximately -2.3 and -3.2 respectively. The first striking feature in this plot is that the continuous acoustic waveform recorded at rupture in the case of the marble (Figure 6a) shows that the peak differential stress cannot be correlated to any particular acoustic emissions. Brittle failure therefore seems to have initiated aseismically—at least in the ultrasonic experimental frequency range, i.e. 0.1–1 MHz.One should note, however, that, as the slip accelerated during the latter phase of rupture propagation and/or frictional sliding, the amount of recorded acoustic activity increased, which might be due to the shearing of asperities. This recording thus corresponds to the aseismic/seismic transition, which occurs for slip rates of the order of mm/s in carbonate rocks at room temperature.

Interestingly, rupture radiated very little energy compared to what is typically observed on intact silicastic rocks such as sandstones. For comparison, Figure 6b displays the acoustic activity recorded at failure in an intact sample of 14% porosity Fontainebleau sandstone deformed in similar conditions. The recorded energy is one and a half orders of magnitude larger than for the marble sample, although the calculated moment magnitude is equal to -3.2 (equivalent to a 200 μm slip only compared to 1.5mm in the case of the marble), i.e. almost one order of magnitude lower. Attenuation and scattering, larger in the sandstone, cannot be responsible for the major differences in the two recordings. These differences can only be qualitatively understood when considering that: 1) the critical stress intensity factor of quartz ($\sim 1MPa.m^{1/2}$) is one order of magnitude larger than that of pure calcite ($\sim 0.2MPa.m^{1/2}$); 2) in the case of a purely brittle material such as Fontainebleau sandstone, the elastic energy at stress drop is released instantaneously (< 0.1 s). This energy is then partially converted into radiated energy at the crack tip and the maximum radiated acoustic energy thus clearly correlates to the peak stress. In the case of ductile failure as in the marble, dislocation and twin accumulation is such that crack propagation steps are small and/or slow, and

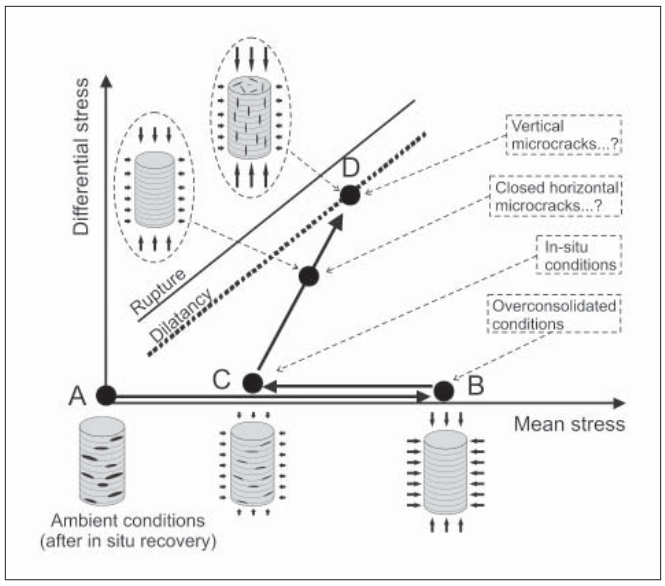

Figure 7. *Loading path for the three experimental data sets: (i) First data set at ambient conditions ≡ A ; (ii) Second data set under isotropic stress ≡ A-B-C ; (iii) third data set under axial stress applied perpendicular to the bedding plane in two successive cycles ≡ C-D-C-D-C. (from Sarout and Guéguen 2008.)*

thus the radiated energy release rate remains small at early stages of rupture and increases with rupture speed. At early stages of rupture, the radiated energy might also be absorbed by neighboring dislocations and/or intermittent dislocation flow. This last observation clearly highlights the dependence of radiated acoustic (and microseismic?) energy during crack propagation not only on the rupture propagation speed and the slip velocity but most importantly on the rock's lithology and rheology. This could have important implications as carbonates are prevalent within sedimentary basins and oil fields. At even shallower depths and prevalent within fault gouges, clay minerals are also expected to behave in a similar way.

Where does shale elastic anisotropy come from?

In contrast to sandstones, shales are very fine-grained sedimentary rocks. Grain contacts transmit the load in the case of sandstones, whereas the clay matrix supports the load in the case of shales. Also in contrast to sandstones, shales are fairly anisotropic rocks. In general, rock anisotropy is the combined result of two factors: mineral grains preferred orientation and oriented low-aspect ratio pores (crack-like pores). At high effective pressure, this second effect is expected to progressively vanish, as crack closure pressure is of the order of (aspect ratio) × (Young modulus). Depending on the exact values of these quantities, the closure pressure is expected to be in the range 20–100 MPa for shales. The first effect, due to mineral preferred orientation, is not expected to depend significantly on pressure. Figure 7 shows the effect of isotropic and deviatoric stresses on a cylindrical shale specimen cored perpendicular to the rock bedding plane.

Experiments conducted on dry and wet Bure shale samples (a Callovo-Oxfordian shale from about 500 m depth, investigated by the French agency for radioactive waste management ANDRA) have evidenced a clear variation of

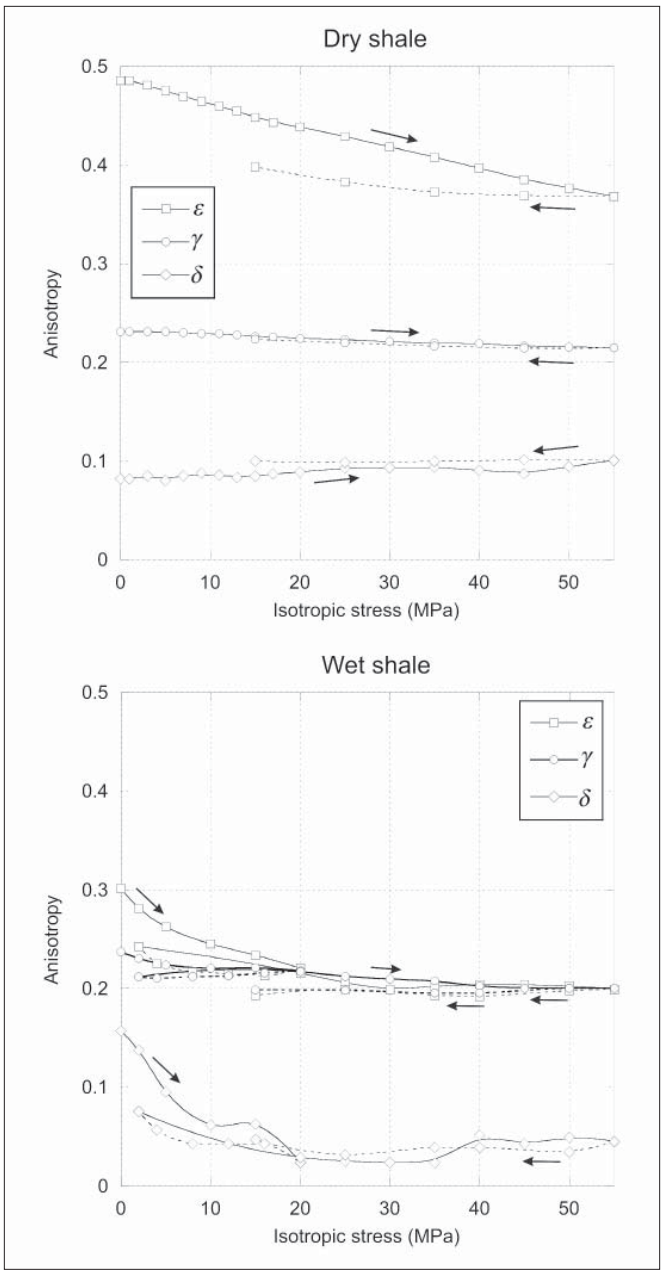

Figure 8. *Evolution of dry and wet (undrained) Bure shale anisotropy under isotropic stress. (——) loading ; (- - -) unloading. (from Sarout and Guéguen 2008.) The plot shows the three Thomsen parameters* ε, γ, δ.

elastic anisotropy with confining pressure (Figure 8). Assuming transverse isotropy (TI), and using Thomsen parameters ε, γ, δ to quantify anisotropy, the elastic anisotropy is found to decrease between Pc = 0, (ε= 0.5) and Pc = 55 MPa, (ε= 0.37) in the dry case. In the wet case, ε decreases from 0.3 to 0.2 under similar conditions. Although the experiments have not explored the domain of higher confining pressures (beyond 55 MPa), it seems that anisotropy does not vanish at high confining pressure. This is expected as a fraction of anisotropy is the result of preferred orientation of clay particles. The observed strains associated with ε variations are very small, close to 0.5%. It does not seem possible to explain the observed elastic properties variations if compliant pores

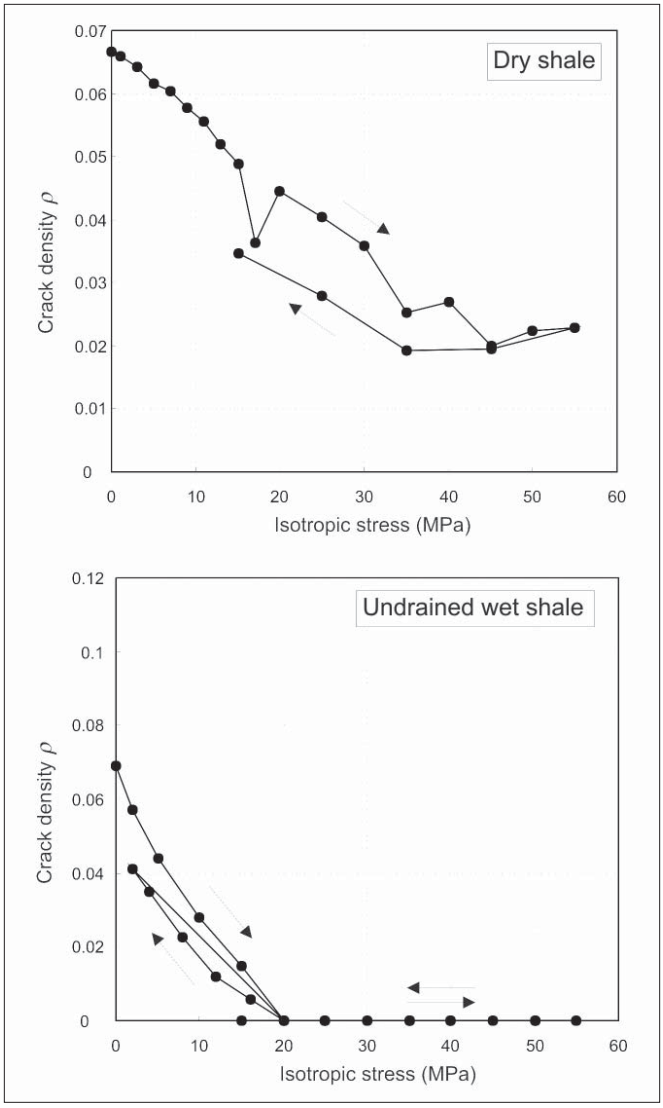

Figure 9. *Evolution of (horizontal) crack density ρ with isotropic stress in a dry (top) and in an undrained wet shale (bottom). In the dry case, the crack density ρ decreases from 0.07 towards 0.02 when confining pressure is increased from 0 to 55 MPa. In the undrained wet case, crack density ρ decreases from 0.07 towards 0 when confining pressure is increased from 0 to 20 MPa. Some hysteresis is associated with unloading in both cases. (from Sarout and Guéguen 2008, Figures 4b and 6b.)*

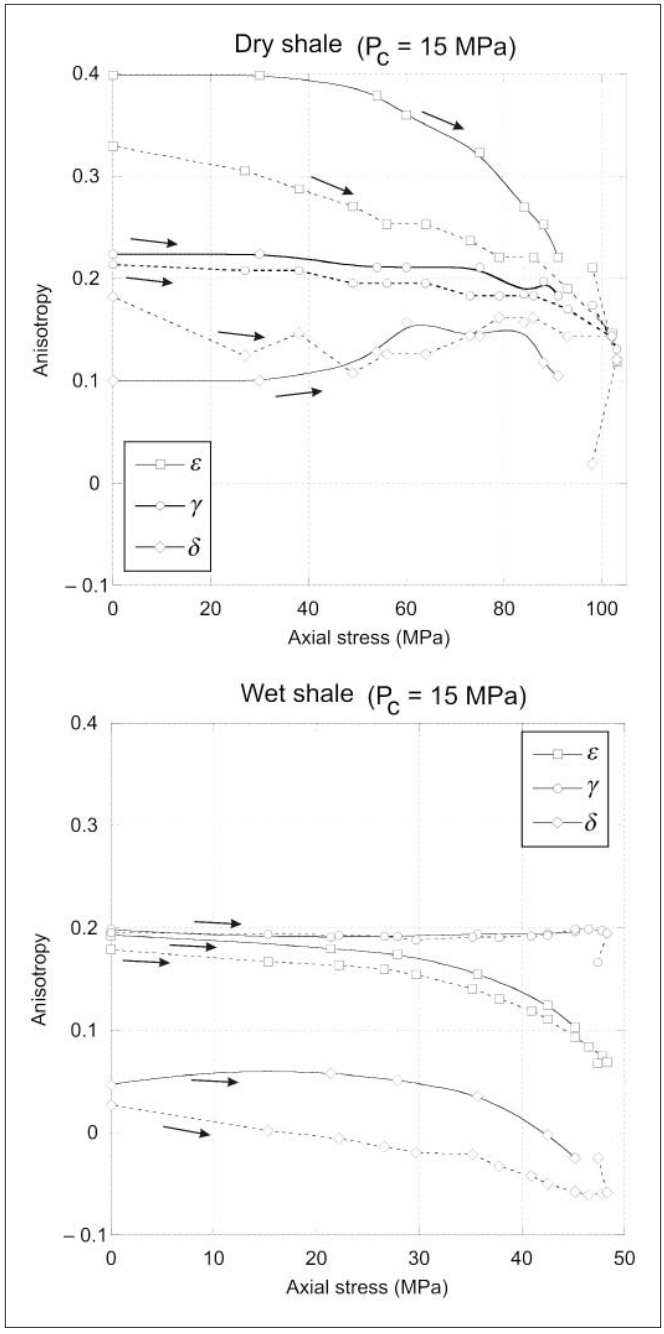

Figure 10. *Evolution of dry and wet (undrained) shale anisotropy under confining pressure of 15 MPa and axial stress applied perpendicular to the rock bedding plane. (—) first loading; (—) second loading. (from Sarout and Guéguen 2008, Figure 16.)*

(low-aspect ratio pores) are not considered. Only such crack-like pores can produce effective elastic property variations with very small porosity changes. Using effective elasticity, it is possible to invert the elastic wave velocity data to get crack density, as in the case of sandstones. There is however an additional complexity that is linked to anisotropy. To overcome this difficulty, a minimalist approach can be followed, that assumes crack-like pores to be embedded in a TI matrix. The matrix contains all solid phases together with equant porosity. Full analytical solutions are known for crack-like pores embedded in a TI matrix in only one case: that of a crack (or an ellipsoidal pore) aligned in the TI symmetry plane. Indeed this situation is an excellent first order approximation for the case we are interested in. It is likely that crack-like pores are more or less oriented along clay particles interfaces. Using the above described approach, the data in the dry case are consistent with an initial crack density of 0.07, decreasing to 0.02 at 55 MPa. In the wet case, crack density decreases to zero (Figure 9).

Anisotropic loading, as in the case of sandstones, modifies strongly shale properties. Deviatoric stresses have a clear effect on ε, γ, δ variations. A prefailure drop of ε is observed both in the dry and wet cases (Figure 10). Inverting the velocity data, crack density in the TI symmetry plane is observed to decrease, in the dry case, from 0.07 to 0.04. In the wet case, the inverted crack density values are very low up to close to

failure where they increase strongly. However, it is likely that, at that point, the model is no longer valid. This is because cracks are assumed to be lying in the TI symmetry plane, whereas perpendicular cracks probably develop close to failure (Figure 11).

From laboratory scale to field scale: heterogeneity and frequency effects

How reliable is the extrapolation of laboratory data, such as those discussed above, to the field scale? Rocks are heterogeneous at all scales so that the use of effective elasticity must be questioned. Obviously, if the degree of heterogeneity remains small, i.e., if heterogeneity results mainly from small composition and porosity variations, applicability of effective elasticity and extrapolation of laboratory data to field scale is acceptable. For a given rock type corresponding to a given layer at depth, laboratory results provide useful guidelines.

There is, however, another reason that may prevent a direct extrapolation from laboratory to field scale, if elastic wave velocities are involved. In general, the porous rocks we are interested in may contain a fluid, in which case frequency effects may exist. Laboratory data are obtained in the ultrasonic range, typically in the range of 1 MHz frequency. Given the extremely small value of the wave period (1 microsecond), it is not possible for the fluid pressure to reach equilibrium within one period time, either at the microscale (i.e., between two neighboring cracks or pores), or at the scale of the representative volume element (RVE). Because cracks of different orientations have different compliances, fluid pressure is different in different cavities depending on aspect ratio (geometry) and orientation (unrelaxed state). This effect is negligible for a gas, but it is not for viscous liquids, due to their difference in compressibility (squirt flow effect). The situation is that of a non-isobaric state at the RVE scale. The use of effective elasticity is indeed in agreement with such a situation: effective elasticity describes a non-isobaric situation, even at the microscale. This is why effective elasticity is appropriate to interpret laboratory data similar to those discussed above. However, a question remains, that is: what about field data obtained using seismic or seismological methods at much lower frequencies (kHz, Hz)? They cannot be a priori directly compared to high frequency laboratory data.

In fact, at lower frequencies, fluid pressure can be equilibrated at the RVE scale because fluid has enough time to flow (at least over a short distance such as the RVE scale). This corresponds to an isobaric (relaxed) state. Then effective elasticity does not apply. Instead, poroelasticity (Biot theory) is the relevant theoretical tool that should be used. The two key questions are: (1) what is the critical frequency for the transition? and, (2) what is the possible magnitude of this effect? An approximate answer to the first question is given by the critical frequency value $f_c \sim A^3E/20\eta$ where A is the crack aspect ratio, E the rock Young modulus, and η the fluid viscosity. The key factor is the aspect ratio A. Local flow (within a RVE) does not depend on macroscopic permeability, but on local pore aperture. The A^3 dependence reflects a crack aperture cubed dependence. For instance, using $A = 10^{-3}$, E = 70 GPa, $\eta = 10^{-3}$ Pa.s, one gets $f_c \sim 3.5$ kHz. As a consequence, it is likely that in the case of sandstones laboratory data are in the unrelaxed state, while field data are in the relaxed one. In the case of shales, Young's modulus is variable. Laboratory data are in an unrelaxed state, and field data could be in a relaxed or unrelaxed state. In order to answer the second question, Thomsen parameters have been theoretically derived using both effective elasticity and poroelasticity. In such a case (cracks of different orientations), the crack density tensor α should be used instead of the scalar crack density ρ. Moreover a second, fourth-rank tensor β is also required to completely describe crack density (Sayers and Kachanov, 1995). The results of Figure 12 show that for a sandstone, predicted relaxed and unrelaxed elastic anisotropies can be very different.

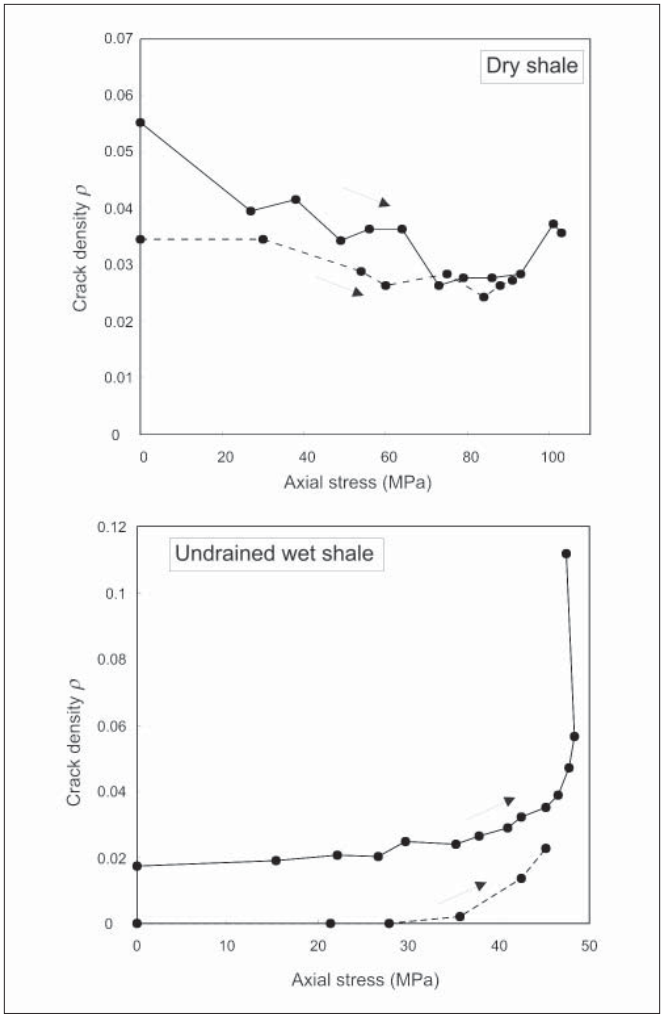

Figure 11. *Evolution of (horizontal) crack density ρ with deviatoric stress in a dry shale (top) and in an undrained wet shale (bottom). The first loading is indicated in dashed line (- - -) and the second loading by a straight line (——). In the dry case, crack density ρ decreases from 0.05 towards 0.025 when axial stress is increased from 0 towards 90 MPa, then it increases significantly after this threshold to eventually reach 0.04 around sample rupture. After the first loading, a larger crack density is observed. In the undrained wet case, crack density ρ remains more or less constant until axial stress reaches 35 MPa, then increases drastically until peak axial stress is reached. Irreversible crack-density increment is observed between the two axial loading cycles. (from Sarout and Guéguen 2008b, Figures 5b and 7b.)*

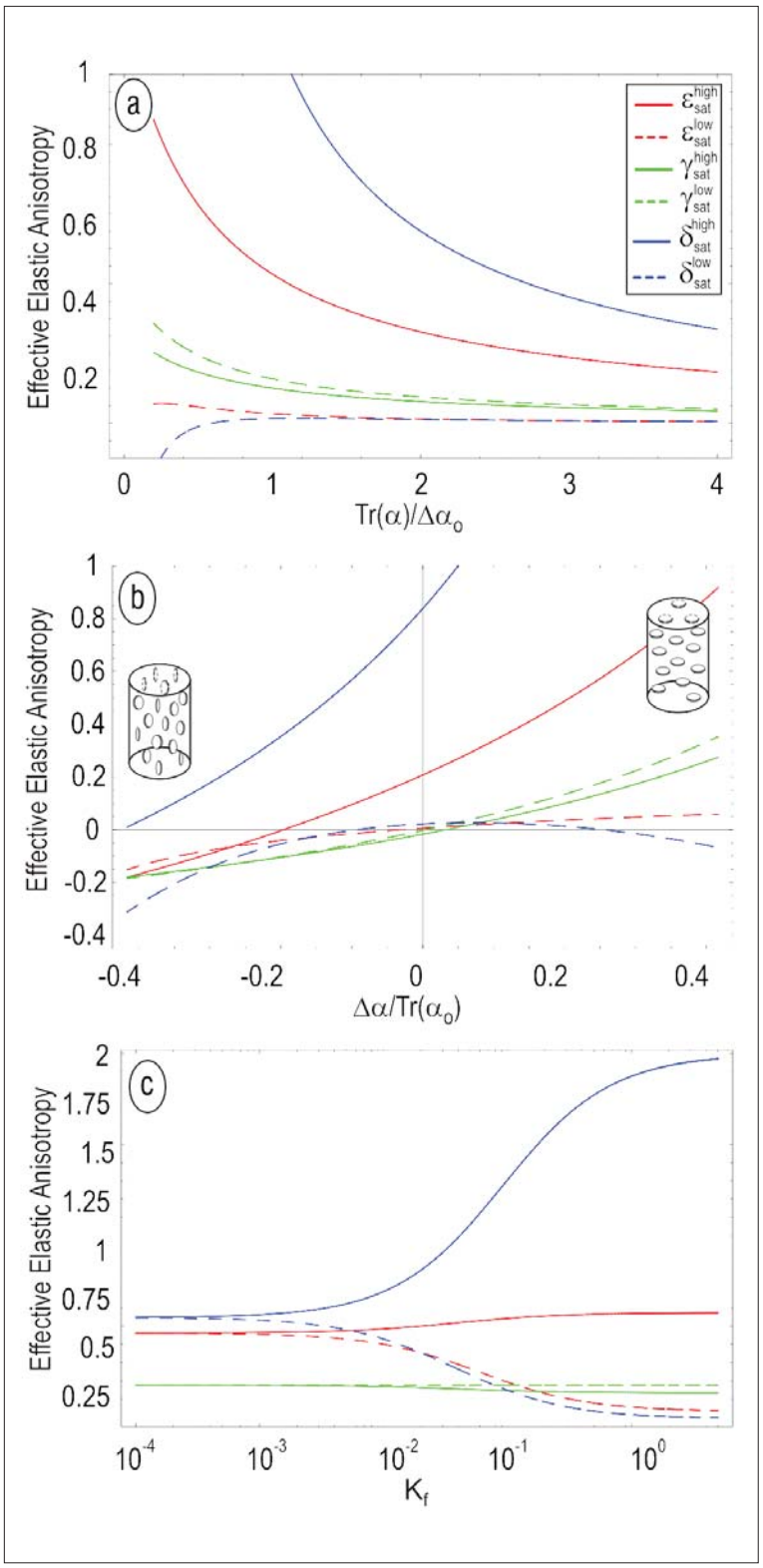

Figure 12. *Comparison of relaxed (low frequency, dashed lines) and unrelaxed (high frequency, plain lines) elastic anisotropies of a fluid-saturated cracked sandstone. Crack density is* $\rho = Tr(\alpha)$ *where* α *is the crack density tensor. Anisotropy of crack distribution is quantified by* $\Delta\alpha = (\alpha_{11} - \alpha_{33})$. *Kf is the fluid bulk modulus.* (E_0 = 70 GPa, ν_0 = 0.27, K_f = 2.3 GPa, $Tr(\alpha_o)$ = 0.6 and $\Delta\alpha_o$ = 0.25, β_{1111} = -0.1, β_{1133} = -0.3, β_{3333} = -0.025). *(from Guéguen and Sarout 2008, Figure 3.)*

Conclusions

The simultaneous measurement of mechanical behavior (stress-strain plots), acoustic emissions, and elastic wave velocities (including anisotropy) is of great interest for both fundamental understanding of rock physical/mechanical properties and geophysical applications. Before failure takes place, damage develops through cracking. This modifies the elastic wave speeds. Very different rocks, such as sandstones, marbles and shales, show very different acoustic signatures at rupture and have been investigated using these methods.

We have shown that sandstone compaction is taking place through cracking, and accordingly exhibits a clear velocity drop, both for V_P and V_S, to gether with an increase in V_P/V_S ratio (both in dry and wet samples). In the case of shales, anisotropy is partly due to crack-like pores that are very sensitive to mean pressure and to deviatoric stress.

Suggested reading. "Microcracks-induced elastic wave anisotropy of brittle rocks" by Sayers and Kachanov (*JGR*, 1995). "The transition from brittle faulting to cataclastic flow in porous sandstones." by Wong et al. (*JGR*, 1997). "Stress-dependent seismic anisotropy of shales" by Sayers (Geophysics, 1999). "Seismic anisotropy of shales" by Sayers (SEG 2004 *Expanded Abstracts*). Elastic wave velocities and permeability evolution during compaction of Bleuswiller sandstone" by Fortin et al. (*International Journal of Rock Mechanical and Mineral Sciences,* 2005). "Acoustic emission and velocities associated with the formation of compaction bands in sandstone" by Fortin et al. (*JGR*, 2006). "Effect of pore collapse and grain crushing on ultrasonic velocities and V_P/V_S" by Fortin et al. (*JGR*, 2007). "Transient creep, aseismic damage and slow failure observed around the brittle ductile transition of Carrara marble" by Schubnel et al. (*GRL* 2006). "Pore pressure induced rupture and aftershocks on intact Fontainebleau sandstone in the laboratory" by Schubnel et al., (*GRL* 2007). "Anisotropy of elastic wave velocities in deformed shales: Part I—Experimental results." by Sarout and Guéguen (Geophysics, 2008). "Anisotropy of elastic wave velocities in deformed shales: Part II — Modeling results" by Sarout and Guéguen (Geophysics, 2008). "Crack-induced anisotropy in crustal rocks: predicted dry and fluid-saturated Thomsen's parameters" by Guéguen and Sarout (*Physics of the Earth and Planetary Interiors,* 2008). TLE

Acknowledgments: This work has been supported by the CNRS, the French Ministry of Foreign Affairs, ANDRA, Ecole Normale Supérieure, and BP America Inc.

Corresponding author: yves.gueguen@ens.fr